**IPEM** Institute of Physics and Engineering in Medicine
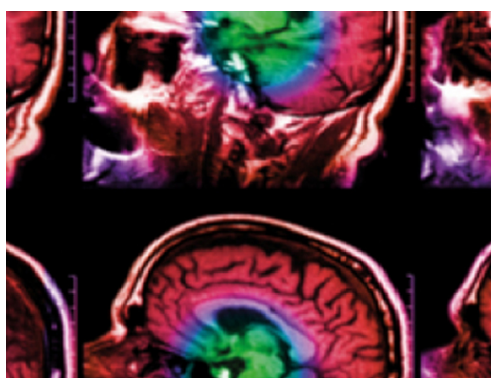
**PAPER**

# A novel method for calibrating head models to account for variability in conductivity and its evaluation in a sphere model

View the article online for updates and enhancements.

**IPEM | IOP**

Series in Physics and Engineering in Medicine and Biology

Your publishing choice in medical physics, biomedical engineering and related subjects.

Start exploring the collection–download the first chapter of every title for free.

# Physics in Medicine & Biology

IPEM Institute of Physics and Engineering in Medicine

**PAPER**

# A novel method for calibrating head models to account for variability in conductivity and its evaluation in a sphere model

S Schrader[1] , M Antonakakis[1,2] , S Rampp[3,4] , C Engwer[5] and C H Wolters[1,6]

[1] Institute for Biomagnetism and Biosignalanalysis, University of Münster, Münster, Germany
[2] Digital Image and Signal Processing Laboratory, School of Electrical and Computer Engineering, Technical University of Crete, Chania, Greece
[3] Department of Neurosurgery, University Hospital Erlangen, Erlangen, Germany
[4] Department of Neurosurgery, University Hospital Halle (Saale), Halle (Saale), Germany
[5] Department of Applied Mathematics, University of Münster, Münster, Germany
[6] Otto Creutzfeldt Center for Cognitive and Behavioral Neuroscience, University of Münster, Münster, Germany

**E-mail:** sophie.schrader@wwu.de

## Abstract

The accuracy in electroencephalography (EEG) and combined EEG and magnetoencephalography (MEG) source reconstructions as well as in optimized transcranial electric stimulation (TES) depends on the conductive properties assigned to the head model, and most importantly on individual skull conductivity. In this study, we present an automatic pipeline to calibrate head models with respect to skull conductivity based on the reconstruction of the P20/N20 response using somatosensory evoked potentials and fields. In order to validate in a well-controlled setup without interplay with numerical errors, we evaluate the accuracy of this algorithm in a 4-layer spherical head model using realistic noise levels as well as dipole sources at different eccentricities with strengths and orientations related to somatosensory experiments. Our results show that the reference skull conductivity can be reliably reconstructed for sources resembling the generator of the P20/N20 response. In case of erroneous assumptions on scalp conductivity, the resulting skull conductivity parameter counterbalances this effect, so that EEG source reconstructions using the fitted skull conductivity parameter result in lower errors than when using the standard value. We propose an automatized procedure to calibrate head models which only relies on non-invasive modalities that are available in a standard MEG laboratory, measures under *in vivo* conditions and in the low frequency range of interest. Calibrated head modeling can improve EEG and combined EEG/MEG source analysis as well as optimized TES.

## 1. Introduction

The distribution of electric activity in the head strongly depends on the geometric and conductive properties of the head tissues. Understanding these volume conduction effects is crucial for many applications in neuroscience, such as electroencephalography (EEG), combined EEG and magnetoencephalography (MEG) and transcranial electric stimulation (TES) (Brette and Destexhe 2012, Bikson *et al* 2016). To address this aspect, magnetic resonance imaging (MRI) has been widely used to create more realistic head volume conductor models by segmenting the head into several tissues. Typically, literature values are used to assign conductivities to these tissue compartments.

Although the conductivities of most head tissues are subject to a relatively high uncertainty, the skull seems especially important due to its high resistivity and considerable influence on the electric forward solutions. Sensitivity studies of EEG and TES forward and inverse problems have highlighted the importance of skull conductivity and the skull/scalp conductivity ratio (Vorwerk *et al* 2019, Vallaghé and Clerc 2009, Saturnino *et al* 2019, Schmidt *et al* 2015). Consequently, variations in skull modeling and conductivity have a strong effect on source reconstruction and TES, e.g. shown in simulations in spherical and realistic models

(Chen *et al* 2010, Montes-Restrepo *et al* 2014, Roche-Labarbe *et al* 2008, Saturnino *et al* 2019, Schmidt *et al* 2015) or in the context of localizing interictal spikes in epilepsy diagnosis (Aydin *et al* 2017).

It is assumed that the skull conductivity strongly varies inter- and intra-individually, e.g. based on age (Antonakakis *et al* 2020, Hoekema *et al* 2003, Wendel *et al* 2010). Different measurement techniques such as electrical impedance tomography (Abascal *et al* 2008, Fernández-Corazza *et al* 2018, Nissinen *et al* 2015), directly applied current (Akhtari *et al* 2002, Hoekema *et al* 2003, Tang *et al* 2008) and magnetoacoustic tomography (Li *et al* 2016) have been proposed and used to individually estimate this parameter. In combination with different measurement conditions (e.g. different temperature or frequency, *in vivo/in vitro* samples) and skull tissue modeling assumptions, a recent review by McCann *et al* (2019) found highly varying literature values for bulk skull conductivities with a weighted mean of 0.016 S m$^{-1}$ based on the reliability rating of the study results. Similarly varying values have been reported for the brain-to-skull conductivity ratio (Lai *et al* 2005, Gonçalves *et al* 2003, Baysal and Haueisen 2004).

Therefore, an individual calibration of the head volume conductor model with respect to skull conductivity has been suggested. There have been several attempts to estimate skull conductivity from EEG alone (Akalin Acar *et al* 2016, Lew *et al* 2009). However, due to its complementarity and its insensitivity to skull and skin conductivity, additional MEG stabilizes the skull conductivity estimation procedure (Antonakakis *et al* 2020, Gonçalves *et al* 2003, Baysal and Haueisen 2004, Huang *et al* 2007, Wolters *et al* 2010, Fuchs *et al* 1998). These studies rely on recorded somatosensory evoked potential (SEP) and field (SEF) data, where the underlying source of the P20/N20, i.e. the component at 20 ms post-stimulus, is mainly of lateral, focal, single dipolar origin and tangential orientation (Nakamura *et al* 1998, Allison *et al* 1991, Götz *et al* 2014, Antonakakis *et al* 2019, 2020).

In this work, we present a new pipeline for volume conductor calibration by means of individual skull conductivity estimation in a continuous parameter space. Our method is only relying on non-invasive modalities that are available in a standard MEG laboratory. It measures under *in vivo* conditions and in the low frequency range of interest, when considering the frequency-dependence of conductivity measurements (Stinstra and Peters 1998, Akhtari *et al* 2002, Tang *et al* 2009). Using individually measured P20/N20 SEP and SEF topographies, it estimates the most influential head model conductivity parameter, namely skull conductivity (Vorwerk *et al* 2019, Saturnino *et al* 2019, Schmidt *et al* 2015), together with the underlying source. This so-called calibrated head model can then be used for the evaluation of EEG or combined EEG/MEG data of interest, for example in presurgical epilepsy diagnosis (Aydin *et al* 2017), as well as to individually optimize multi-channel TES montages (Saturnino *et al* 2019, Huang *et al* 2017, Guler *et al* 2016, Schmidt *et al* 2015, Sadleir *et al* 2012).

Our calibration algorithm exploits the complementarities of EEG and MEG and builds upon already existing calibration methods such as (Aydin *et al* 2014, Antonakakis *et al* 2019, 2020). In these calibration approaches, a discrete set of possible skull conductivity values is used, which limits the accuracy of the algorithm if the optimum lies in between these values. In (Aydin *et al* 2014), for instance, 11 discrete values for the skull conductivity were used, while in (Antonakakis *et al* 2019, 2020), 14 discrete values were used by individually choosing further values around the expected optimal value. In addition, the studies mentioned above use a time-consuming manual calibration procedure involving different toolboxes, e.g. SimBio[5] for the forward calculations and Curry[6] for dipole scans.

In this work, we present a calibration procedure which calibrates the head model with respect to the most influential parameter skull conductivity using a continuous parameter space. Additionally, by providing a complete mathematical description and an optimization method to automatically update the skull conductivity parameter iteratively in order to find the best fitting value, we allow an automated and accurate calibration procedure which can easily be integrated into existing analysis pipelines.

Moreover, in Aydin *et al* (2014), and Antonakakis *et al* (2019, 2020), their calibration algorithm was applied to some realistic cases without estimating its reliability. In this study, we explicitly use a controlled scenario of the multi-layered sphere model, where (quasi-)analytic forward modeling solutions exist. Therefore, we can systematically quantify the errors without interplay with numerical errors that are unavoidable in realistic head modeling setups. We investigate the effects of different levels of noise and of inaccurate assumptions on skin conductivity. Moreover, we analyze the accuracy of the method with regard to different dipole eccentricities and orientations in order to investigate the option of calibrating using other than somatosensory sources, although the focus lies on dipole characteristics corresponding to the P20/N20 component of somatosensory evoked responses.

Results indicate that the reference skull conductivity can be reliably reconstructed for sources similar to the generator of the P20/N20 response. If wrong assumptions are made for the scalp conductivity, the

---

**Table 1.** Four compartment sphere model (Akhtari *et al* 2002, Ramon *et al* 2004, Hoekema *et al* 2003, Haueisen *et al* 1997, Aydin *et al* 2014, Antonakakis *et al* 2020).

| Tissue | Radii (mm) | Conductivity (S m$^{-1}$) |
| --- | --- | --- |
| Scalp | 89.1 | 0.43 |
| Skull | 83.3 | 0.01 (reference) |
|  |  | (0.0008, 0.033) (optimization) |
| CSF | 77.5 | 1.79 |
| Brain | 75.6 | 0.33 |

algorithm results in a skull conductivity parameter which counterbalances this effect, so that EEG source reconstructions using the calibrated skull conductivity result in lower errors than when using standard skull conductivity.

## 2. Methods

### 2.1. Spherical head model and sensor setup

For the simulations, a concentric sphere model was used consisting of 4 layers, which correspond to scalp, skull, cerebrospinal fluid (CSF), and brain tissue. A least-squares fit was used to fit a standard sphere model with radii of 78, 80, 86 and 92 mm to the electrode positions of a subject who participated in a somatosensory experiment, keeping the ratios between the radii unchanged. The resulting sphere model parameters are summarized in table 1. For the MEG sensor positions and orientations, the realistic sensor setup (CTF, VSM MedTech Ltd) of this measurement was used consisting of 271 first-order axial gradiometers and 13 reference coils. The spherical head model with the EEG/MEG sensors is visualized in figure 1(a).

### 2.2. Test dipole characteristics

The characteristics (location, orientation, strength) of the test dipoles used in the simulations are based on source reconstructions of the somatosensory P20/N20 response in realistic head models. Three different stimulation techniques were investigated for five subjects in Antonakakis *et al* (2019): electric stimulation of the median nerve at the wrist (EW), and tactile stimulation of the distal phalanx of the index finger using either a pneumatic membrane (PT) or a Braille stimulator (BT). The average reconstructed P20/N20 dipole strength of the SEP and SEF response in a six compartment realistic head model was 4.7 μAmm ± 2.2 μAmm (PT), 9.7 μAmm ± 6.0 μAmm (BT) and 25.1 μAmm ± 6.5 μAmm (EW) for the three stimulation types. Furthermore, in a follow-up study in a group of 20 subjects, we observed mean source depths of 15.5 mm ± 4.5 mm relative to the inner skull surface (Antonakakis *et al* 2020). The sources were rather tangentially oriented with a mean elevation angle towards the radial orientation of 25.5° ± 18.6°, the largest outlier was observed with 65°. As test dipole locations, 500 randomly positioned points at eight different eccentricities ranging from 0.2 to 0.982 relative to the inner sphere surface were constructed within the upper half of the spherical model. This includes the eccentricity of 0.821, which corresponds to a distance of approx. 15.5 mm to the inner skull surface to simulate realistic P20/N20 source depth (Antonakakis *et al* 2020). Other eccentricities are considered to investigate the performance of the algorithm under more extreme scenarios, e.g. if other sources than the somatosensory evoked P20/N20 response generator are considered that are closer to the region of interest for EEG/MEG source analysis or optimized TES. Additionally, a regular source grid with a resolution of 2 mm was constructed covering the upper half of the brain compartment. Note that the test dipole locations do not coincide with nodes of this source space in order to avoid an inverse crime for inverse reconstructions, i.e. model and reality are identified (Kaipio and Somersalo 2005), as this usually leads to overly optimistic results. On average, the test dipoles are 0.97 mm ± 0.28 mm away from the closest source space node.

For each test dipole position, a random tangential orientation and vectors elevated by 25° and 65° towards the radial direction, were created to simulate the average and the extreme P20/N20 source scenario, both observed in the experiment (Antonakakis *et al* 2019).

In a first comparison, the dipole strengths of the three different stimulation types are compared to each other. For the other test cases, the dipole strength corresponding to EW stimulation was used for the simulations. The test dipole characteristics are visualized in figure 1(b).

### 2.3. Reference EEG and MEG signals with realistic noise levels

(Quasi-)analytical solutions for the EEG and MEG forward problems exist for concentric multi-layer sphere models. For each test dipole, the analytical MEG solution was computed using the closed formula provided
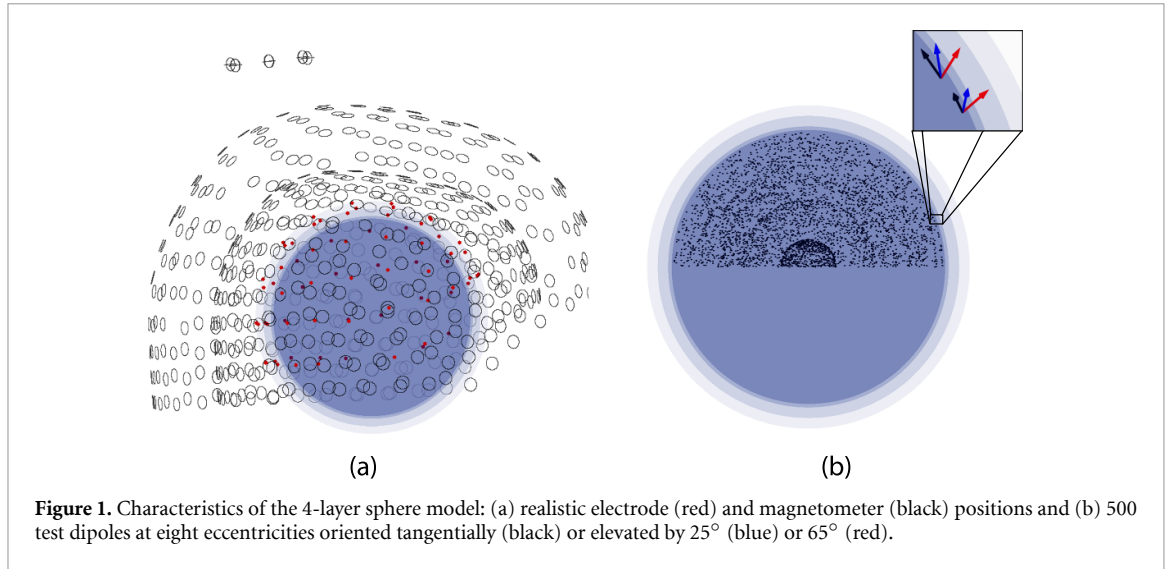
**Figure 1.** Characteristics of the 4-layer sphere model: (a) realistic electrode (red) and magnetometer (black) positions and (b) 500 test dipoles at eight eccentricities oriented tangentially (black) or elevated by 25° (blue) or 65° (red).

---

**Algorithm 1.** Calibration procedure

---

**Input**: $M_{\text{EEG}}$, $M_{\text{MEG}}$, $l_{\text{EEG}}$, $l_{\text{MEG}}$, $\sigma_{\min}$, $\sigma_{\max}$, $\varepsilon$

    **1.** Compute the optimal dipole position from MEG data:

$$x_{\text{MEG}} = \operatorname{argmin}_{x \in S} ||M_{\text{MEG}} - l_{\text{MEG}}(x)\,[l_{\text{MEG}}(x)]^{+}\,M_{\text{MEG}}||_2^2$$

$$L_{\text{MEG},x_{\text{MEG}}} = l_{\text{MEG}}(x_{\text{MEG}})$$

    **2.** Find $\sigma_{\text{skull,est}} = \operatorname{argmin}_{\sigma_{\text{skull}} \in (\sigma_{\min}, \sigma_{\max})} r(\sigma_{\text{skull}})$ using Brent's method, which proposes $\sigma_{\text{skull}}^i$ in iteration
      $i = 0, 1, ...,$ with the residual variance defined as

$$r(\sigma_{\text{skull}}^i) := \frac{||M_{\text{EEG}} - L_{\text{EEG},x_{\text{MEG}},\sigma_{\text{skull}}^i}\,j_{\text{est}}||_2^2}{||M_{\text{EEG}}||_2^2},$$

    where $L_{\text{EEG},x_{\text{MEG}},\sigma_{\text{skull}}^i}$ and the dipole moment $j_{\text{est}}$ are computed as follows:

$$L_{\text{EEG},x_{\text{MEG}},\sigma_{\text{skull}}^i} = l_{\text{EEG}}(x_{\text{MEG}},\sigma_{\text{skull}}^i)$$

$$j_{\text{EEG},x_{\text{MEG}}} = [L_{\text{EEG},x_{\text{MEG}},\sigma_{\text{skull}}^i}]^{+}\,M_{\text{EEG}}$$

$$o_{\text{est}} = \frac{j_{\text{EEG},x_{\text{MEG}}}}{||j_{\text{EEG},x_{\text{MEG}}}||_2}$$

$$m_{\text{est}} = [L_{\text{MEG},x_{\text{MEG}}}\,o_{\text{est}}]^{+} \cdot M_{\text{MEG}}$$

$$j_{\text{est}} = o_{\text{est}} m_{\text{est}}$$

    Terminate iteration, when $\sigma_{\text{skull}}^{i+1} - \sigma_{\text{skull}}^i < \epsilon$.

**Output**: $x_{\text{MEG}}$, $o_{\text{est}}$, $m_{\text{est}}$, $\sigma_{\text{skull,est}}$

---

by (Sarvas 1987). The quasi-analytical EEG solution was computed using the series expansion formulas following (de Munck and Peters 1993).

In order to simulate realistic conditions, in some of the test scenarios noise was added to the (quasi-) analytical solutions using either uncorrelated Gaussian noise or measured baseline signals. The average standard deviation per channel of the baseline signals in the prestimulus interval $[-100\text{ ms}, -5\text{ ms}]$ was computed for five subjects participating in a somatosensory experiment involving electric wrist stimulation in (Antonakakis *et al* 2019). These average standard deviations of noise signals were approximately 0.13 μV for electrodes and 3.2 fT for gradiometers, leading to an average signal-to-noise ratio (SNR) for the P20/N20 response of approximately 5.8 (EEG) and 8.8 (MEG), following the SNR definition of (Fuchs *et al* 1998). In a first noise scenario, white Gaussian noise with the described average strength was added to the (quasi-)analytical EEG and MEG signals. In a second test, signals at random time points within the prestimulus interval $[-100\text{ ms}, -5\text{ ms}]$ of the electric wrist stimulation measurement of one test subject were scaled to match the mean standard deviation observed in the five subjects and added to the (quasi-) analytical solutions. In both cases, a better SNR is achieved for more superficial sources than for deep sources, as it is the case in realistic scenarios.

### 2.4. Algorithm for skull conductivity calibration

The procedure for estimating skull conductivity presented here exploits the different sensitivity profiles of EEG and MEG and is based on the reconstruction of the generator of the SEP/SEF P20/N20 response. In practice, the P20/N20 component of somatosensory evoked responses is well suited, since this early response is extensively studied, indicating a focal and quasi-tangentially oriented dipolar source in Brodmann area 3b (Nakamura *et al* 1998, Allison *et al* 1991, Antonakakis *et al* 2019, Götz *et al* 2014). Thus, it has often been

used for skull conductivity calibration (Aydin *et al* 2014, Huang *et al* 2007, Vallaghé and Clerc 2009, Fuchs *et al* 1998, Antonakakis *et al* 2019, 2020).

In sphere models, where (quasi-)analytical solutions exist, the MEG signal is independent of the conductivity profile of the volume conductor (Sarvas 1987). Also in the realistic case, the MEG forward solution was shown to be insensitive to conductivity changes in the skull and skin compartment (Lew *et al* 2013, Haueisen *et al* 1997). EEG, on the other hand, strongly depends on volume conduction effects and is, from all conductivities, most sensitive to skull conductivity (Vorwerk *et al* 2019). Moreover, there is a strong correlation between skull conductivity and source depth (Chen *et al* 2010, Vorwerk *et al* 2019, Lew *et al* 2009, Akalin Acar *et al* 2016, Huang *et al* 2007, Antonakakis *et al* 2020). When it comes to source orientation, the MEG is blind to radial sources in the analytical sphere model scenario (Sarvas 1987) and insensitive to radial orientation components in the realistic head model (Fuchs *et al* 1998, Antonakakis *et al* 2019, Aydin *et al* 2014).

Based on these strengths and weaknesses of both modalities, the calibration procedure is set up and implemented in a Matlab (R2018a, Natick, Massachusetts: The MathWorks Inc.) pipeline, see algorithm 1. As input, it requires reference data $M_{EEG} \in \mathbb{R}^{s_{EEG}}$, $M_{MEG} \in \mathbb{R}^{s_{MEG}}$, where $s$ denotes the number of sensors for each modality. In practice, these are the measured dipolar P20/N20 responses at the sensors, in our test cases the (quasi-)analytical solutions of test dipoles with location $x_{ref}$, unit length orientation $o_{ref}$ and magnitude $m_{ref}$ are used. All conductivities in the reference volume conductor model are fixed as shown in table 1, except for one test scenario in which $\sigma_{scalp, ref}$ is varied. In most of our validation tests, realistic noise is added to the simulated data, as described in section 2.3. Additionally, functions $l_{EEG} : \mathbb{R}^3 \times \mathbb{R} \to \mathbb{R}^{s_{EEG} \times 3}$, $(x, \sigma_{skull}) \mapsto L_{EEG,x,\sigma_{skull}}$ and $l_{MEG} : \mathbb{R}^3 \to \mathbb{R}^{s_{MEG} \times 3}$, $x \mapsto L_{MEG,x}$ are provided, where $\text{rank}(L_{MEG,x}) = 2$ (Wolters *et al* 1999). These functions $l_{EEG}$ and $l_{MEG}$ compute the EEG and MEG leadfields $L_{EEG,x,\sigma_{skull}}$ and $L_{MEG,x}$, respectively, i.e. the simulated sensor signals for a dipolar source at location x with moments oriented in the three Cartesian directions. These forward calculations are influenced by the head model and sensor characteristics, and in the EEG case also the conductivities, as described in section 2.1. In the realistic case, the leadfields would be computed numerically, in our test scenario, the (quasi-)analytical solutions are used. Additionally, the range $(\sigma_{min}, \sigma_{max})$ for the skull conductivity estimation is defined in table 1 and the convergence tolerance $\varepsilon = 1 \times 10^{-5} \ \text{S m}^{-1}$ is provided.
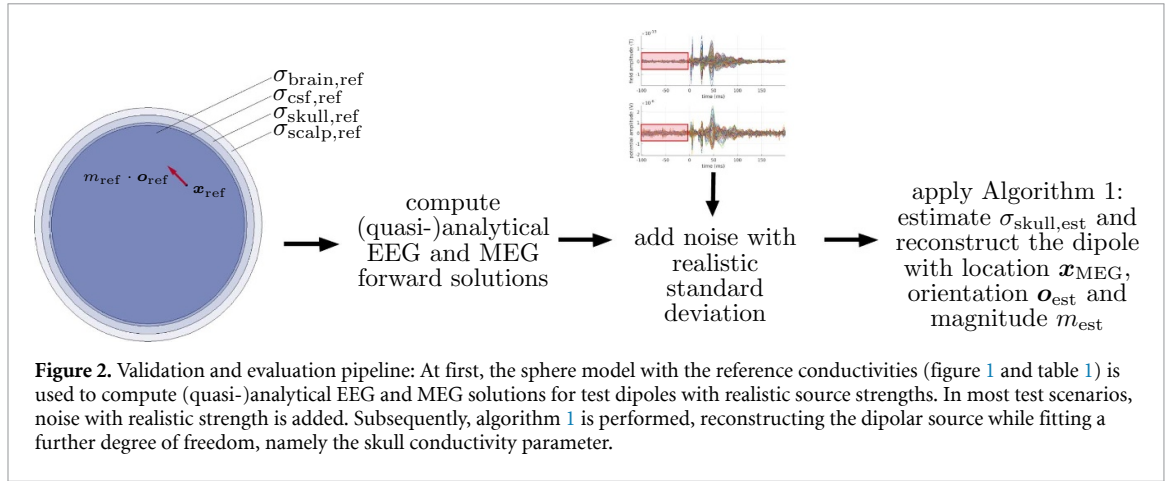
Since the MEG is insensitive to skull conductivity, it has the capability to localize the underlying P20/N20 source in the primary somatosensory cortex with high accuracy, even if skull conductivity is not accurately chosen (Nakamura *et al* 1998, Fuchs *et al* 1998, Aydin *et al* 2014). Therefore, similar to Antonakakis *et al* (2020), Fuchs *et al* (1998), Huang *et al* (2007), Wolters *et al* (2010), Aydin *et al* (2014) and Haueisen *et al* (1997), the MEG is used to fix the location of the P20/N20 source. In step 1, an MEG equivalent current dipole scan is used to find the best fitting source location $x_{MEG}$ within the source space *S*. From here on, **j** denotes the dipole moment and $[\cdot]^+$ the Moore-Penrose pseudo-inverse of a matrix, which in case of the MEG leadfield relies on a truncated singular value decomposition (Wolters *et al* 1999). In step 2, a derivative free minimization method, the so called Brent method (Brent 1972), is used within the Matlab routine *fminbnd* to iteratively perform the steps described below for different skull conductivities $\sigma_{skull}^i$ in the predefined continuous range. The aim is to determine the skull conductivity value which results in the minimal residual variance computed as follows: First, EEG is used for the determination of the source orientation $o_{est}$ using a least squares fit, since EEG is sensitive to both radial and tangential orientation components. The latter is, however, influenced by individual skull conductivity (Vorwerk *et al* 2019). Thus, the source amplitude $m_{est}$ for this fixed source orientation is determined from the MEG again. This is because the tangential component of this source orientation must match the measured MEG, which in turn is insensitive to skull conductivity. Finally, the residual variance is computed between the reference EEG signal and the forward computed EEG for the current skull conductivity and the reconstructed dipole with this fitted orientation and magnitude. These steps are carried out until the tolerance criterion is reached. As a result, the algorithm returns the skull conductivity value $\sigma_{skull,est}$ which best explains the reference data, as well as the estimated source characteristics $x_{MEG}$, $o_{est}$ and $m_{est}$.

In the following, this algorithm is validated and evaluated in a well-controlled forward scenario, namely the multi-layered spherical head model, see figure 2 for an overview of the complete workflow.

## 2.5. Error measures

We evaluate our new calibration algorithm by means of different error measures. First, the relative difference between the estimated and the reference skull conductivity is measured:

$$e_{skull} = 100 \cdot \frac{\sigma_{skull,est} - \sigma_{skull,ref}}{\sigma_{skull,ref}}.$$

**Figure 2.** Validation and evaluation pipeline: At first, the sphere model with the reference conductivities (figure 1 and table 1) is used to compute (quasi-)analytical EEG and MEG solutions for test dipoles with realistic source strengths. In most test scenarios, noise with realistic strength is added. Subsequently, algorithm 1 is performed, reconstructing the dipolar source while fitting a further degree of freedom, namely the skull conductivity parameter.

Note that since we investigate the range of (0.0008, 0.033) S m$^{-1}$ (see table 1) for the skull conductivity, possible values for $e_{skull}$ are within the interval $(-92\%, 230\%)$. In figures 3–7, for the reconstructed dipole, the localization $e_{loc}$ and depth error $e_{depth}$ (mm), where $c$ denotes the center of the sphere, the orientation error $e_{ori}$ (degrees) and the magnitude error $e_{mag}$ (%) compared to the reference dipole are given as

$$e_{loc} = ||\boldsymbol{x}_{MEG} - \boldsymbol{x}_{ref}||_2,$$
$$e_{ori} = \cos^{-1}\left(\boldsymbol{o}_{est} \cdot \boldsymbol{o}_{ref}\right),$$
$$e_{mag} = 100 \cdot \frac{m_{est} - m_{ref}}{m_{ref}},$$
$$e_{depth} = ||\boldsymbol{x}_{MEG} - c||_2 - ||\boldsymbol{x}_{ref} - c||_2.$$

## 3. Results

The algorithm for volume conductor calibration by means of individual skull conductivity estimation was validated and evaluated in the spherical model under different conditions. On average, approximately 11 iterations were required in algorithm 1 until the tolerance criterion was met.

### 3.1. Noise level comparison
In a first test scenario, the (quasi-)analytical solutions were distorted by adding white Gaussian noise with realistic amplitudes. For the tangential test dipoles, the source strengths corresponded to EW, PT and BT as explained in section 2.2.

The results for the reconstructed dipole errors ($e_{loc}$, $e_{ori}$, $e_{mag}$) as well as the overall skull conductivity estimation error $e_{skull}$ are depicted in figure 3. The localization errors (figure 3(a)) as well as the magnitude errors (figure 3(c)), which are related to the MEG signal, are at a low level and nearly constant for more eccentric sources including the practically most interesting eccentricity of 0.821, while they strongly increase for deeper sources. At the most relevant eccentricity of 0.821 when considering the P20/N20 source, the localization errors are at 1.1 mm $\pm$ 0.4 mm (EW), 1.2 mm $\pm$ 0.5 mm (BT) and 1.7 mm $\pm$ 0.8 mm (PT), the magnitude errors at 0.1% $\pm$ 2.6% (EW), 0.02% $\pm$ 3.1% (BT) and 0.3% $\pm$ 4.4% (PT). The dipole orientation errors (figure 3(b)) show a similar trend, although the noise level related to the stimulation types seems to be more influential than the eccentricity. The orientation errors at an eccentricity of 0.821 are 1.1° $\pm$ 0.6° (EW), 2.7° $\pm$ 1.5° (BT) and 5.5° $\pm$ 3.1° (PT). Overall, all error measures increase for lower dipole strengths, as the SNR decreases. The resulting mean skull conductivity errors (figure 3(d)) are 0.06% $\pm$ 5.4% (EW), 1.0% $\pm$ 10.5% (BT) and 3.3% $\pm$ 20.8% (PT) at an eccentricity of 0.821. The SNR (figure 3(e)) increases with source strength and eccentricity and is higher for MEG than for EEG, with mean SNRs of 7.0 (EW), 2.8 (BT) and 1.5 (PT) for EEG and 12.8 (EW), 5.0 (BT) and 2.6 (PT) for MEG at this eccentricity. Note that for the deepest sources at eccentricity 0.2, the MEG least-squares fit in step 2c) in the calibration algorithm results in a negative magnitude, thus flipping the orientation obtained from the EEG fit in step 2b), for 23 (PT) dipoles, resulting in orientation errors of almost 180° (not within the shown range).

In a second scenario, realistic prestimulus noise was added with an identical mean standard deviation. The results for the reconstructed dipole errors ($e_{loc}$, $e_{ori}$, $e_{mag}$) as well as the overall skull conductivity estimation error $e_{skull}$ are depicted in figure 4. The localization errors (figure 4(a)) as well as the magnitude errors (figure 4(c)), which are related to the MEG signal, are again at a low level and constant for more eccentric sources, while they strongly increase for deeper sources.
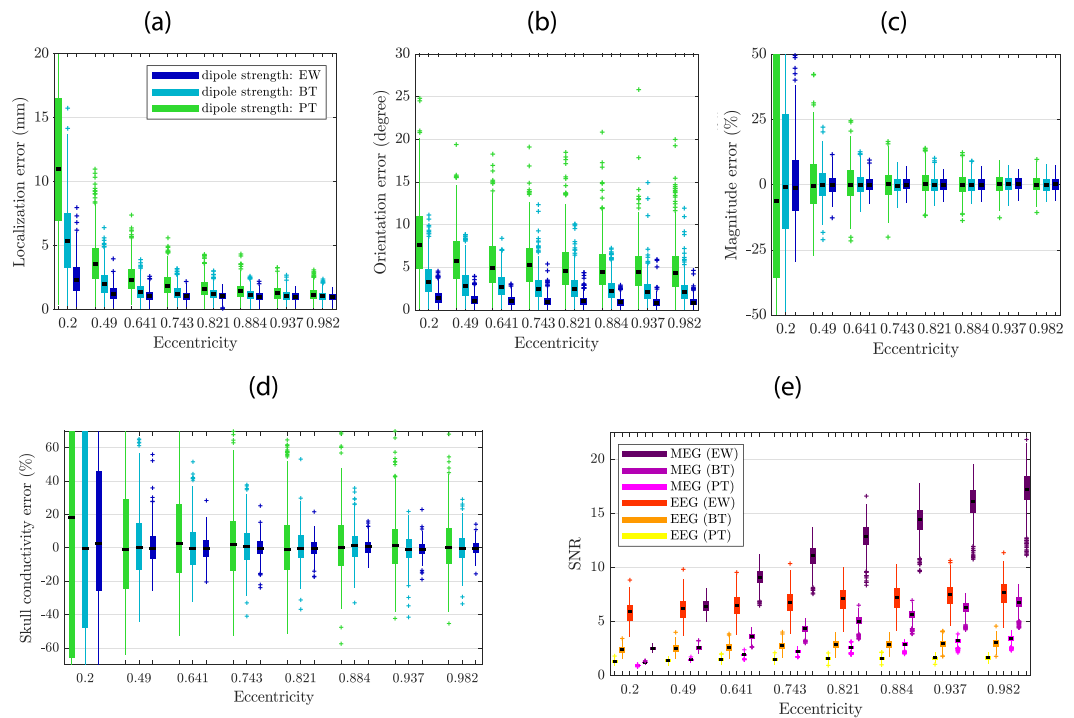
**Figure 3.** Errors in the calibration procedure for tangential sources with magnitudes corresponding to typical values from electric wrist (EW), Braille-tactile (BT) or pneumato-tactile (PT) somatosensory experiments. Source reconstruction errors related to (a) localization, (b) orientation and (c) magnitude, (d) skull conductivity estimation error and (e) SNR of all conditions. As a reference solution, white Gaussian noise with a realistic strength was added to the (quasi-) analytical solutions. The result is shown for test dipoles at different eccentricities plotted on a logarithmic scale. Boxplots show 25th and 75th percentile and median.
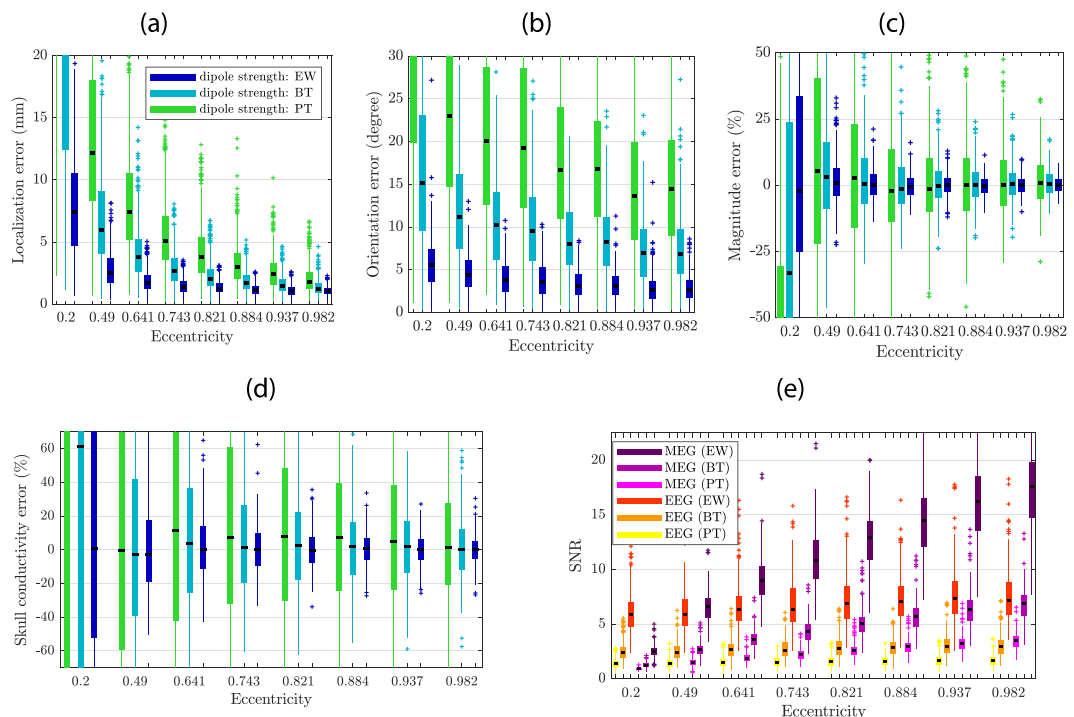


**Figure 4.** Errors in the calibration procedure for tangential sources with magnitudes corresponding to typical values from electric wrist (EW), Braille-tactile (BT) or pneumato-tactile (PT) somatosensory experiments. Source reconstruction errors related to (a) localization, (b) orientation and (c) magnitude, (d) skull conductivity estimation error and (e) SNR of all conditions. As a reference solution, prestimulus noise was added to the (quasi-) analytical solutions. The result is shown for test dipoles at different eccentricities plotted on a logarithmic scale. Boxplots show 25th and 75th percentile and median.
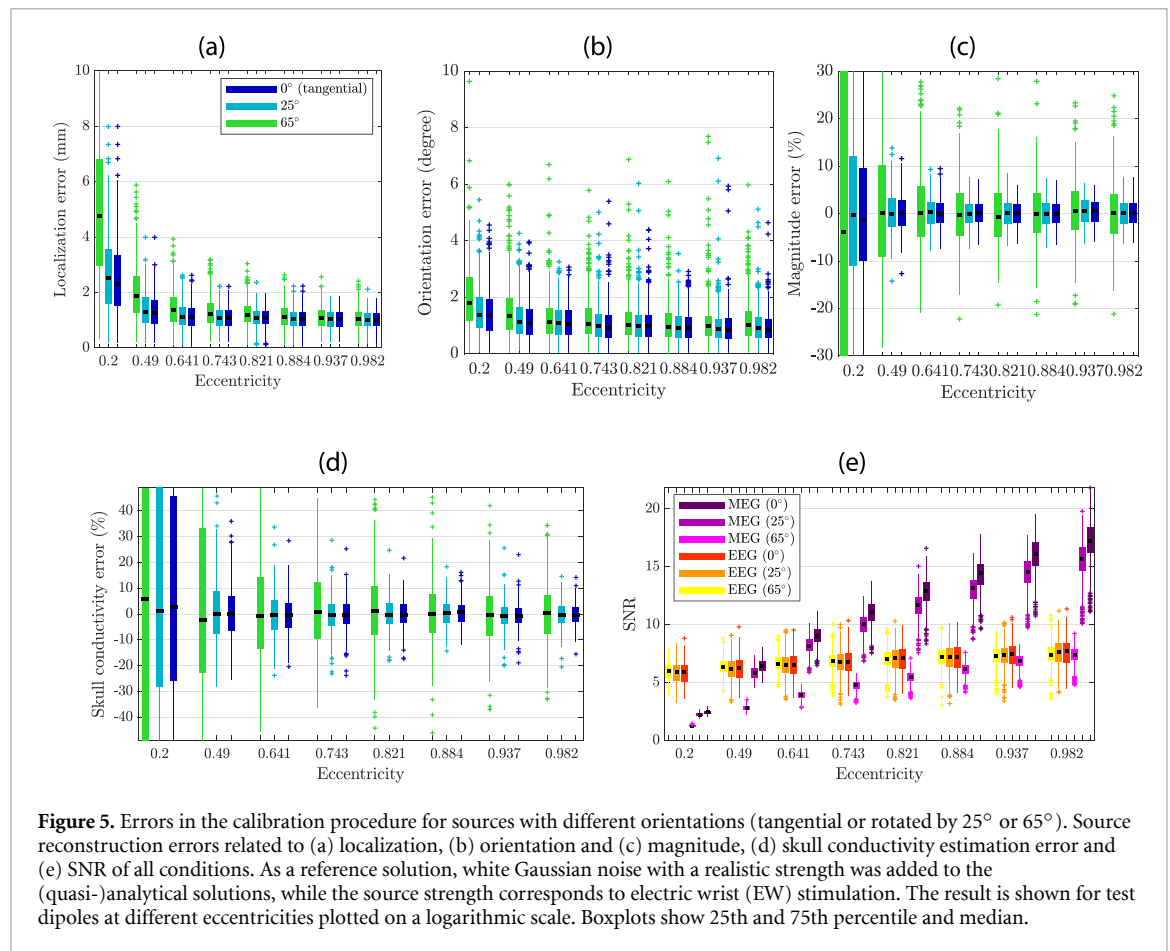
**Figure 5.** Errors in the calibration procedure for sources with different orientations (tangential or rotated by 25° or 65°). Source reconstruction errors related to (a) localization, (b) orientation and (c) magnitude, (d) skull conductivity estimation error and (e) SNR of all conditions. As a reference solution, white Gaussian noise with a realistic strength was added to the (quasi-)analytical solutions, while the source strength corresponds to electric wrist (EW) stimulation. The result is shown for test dipoles at different eccentricities plotted on a logarithmic scale. Boxplots show 25th and 75th percentile and median.

At the most relevant eccentricity of 0.821 when considering the P20/N20 source, the localization errors are at 1.3 mm $\pm$ 0.5 mm (EW), 2.3 mm $\pm$ 1.2 mm (BT) and 4.3 mm $\pm$ 2.7 mm (PT), the magnitude errors at -0.01% $\pm$ 3.9% (EW), 0.2% $\pm$ 8.2% (BT) and 1.4% $\pm$ 18.7% (PT). The orientation errors at an eccentricity of 0.821 are 3.3° $\pm$ 1.7° (EW), 8.6° $\pm$ 4.4° (BT) and 18.0° $\pm$ 9.6° (PT). Overall, all error measures increase for lower dipole strengths, as the SNR decreases. The resulting mean skull conductivity errors (figure 4(d)) are 0.5% $\pm$ 10.9% (EW), 3.5% $\pm$ 28.0% (BT) and 16.1% $\pm$ 60.0% (PT) at an eccentricity of 0.821. The SNR (figure 4(e)) increases with source strength and eccentricity and is higher for MEG than for EEG, with mean SNRs of 7.2 (EW), 2.9 (BT) and 1.6 (PT) for EEG and 12.9 (EW), 5.0 (BT) and 2.6 (PT) for MEG at this eccentricity. Note that the MEG least-squares fit in step 2c) in the calibration algorithm results in a negative magnitude, thus flipping the orientation obtained from the EEG fit in step 2b), for 8 (EW), 85 (BT) and 143 (PT) dipoles at eccentricity 0.2 and 16 (PT) for eccentricity 0.49, resulting in orientation errors of almost 180° (not within the shown range).

Since at the most relevant eccentricity of 0.821, Gaussian noise in combination with EW stimulation leads to overall skull conductivity errors of 0.06% $\pm$ 5.4% which are in a similar low error range, we will proceed in the following with only Gaussian noise scenarios and later discuss how to further optimize our stimulation protocols.

### 3.2. Source orientation comparison

In a second study, the orientation of the test dipoles was varied to investigate the stability of the calibration in case of non-zero radial orientation components of the reference sources in the presence of realistic Gaussian noise levels. For that purpose, each dipole was either fully tangentially oriented or rotated by 25° or 65° out of the tangential plane (see figure 1(b)). Realistic noise levels are used in combination with the source strength resulting in the highest SNR in the previous study (EW). Note that the tangential condition here corresponds to the EW case in the previous section when Gaussian noise is used.

The results for the reconstructed dipole errors ($e_{loc}$, $e_{ori}$, $e_{mag}$) and the overall skull conductivity estimation errors $e_{skull}$ for this test scenario are depicted in figure 5.

At an eccentricity of 0.821, the localization errors (figure 5(a)) are at 1.1 mm $\pm$ 0.4 mm (tangential, 25°) and 1.2 mm $\pm$ 0.5 mm (65°), the magnitude errors (figure 5(c)) at 0.1% $\pm$ 2.6% (tangential), 0.1% $\pm$ 2.9% (25°) and $-0.1\%$ $\pm$ 6.7% (65°). The orientation errors (figure 5(b)) at an eccentricity of 0.821 lie at
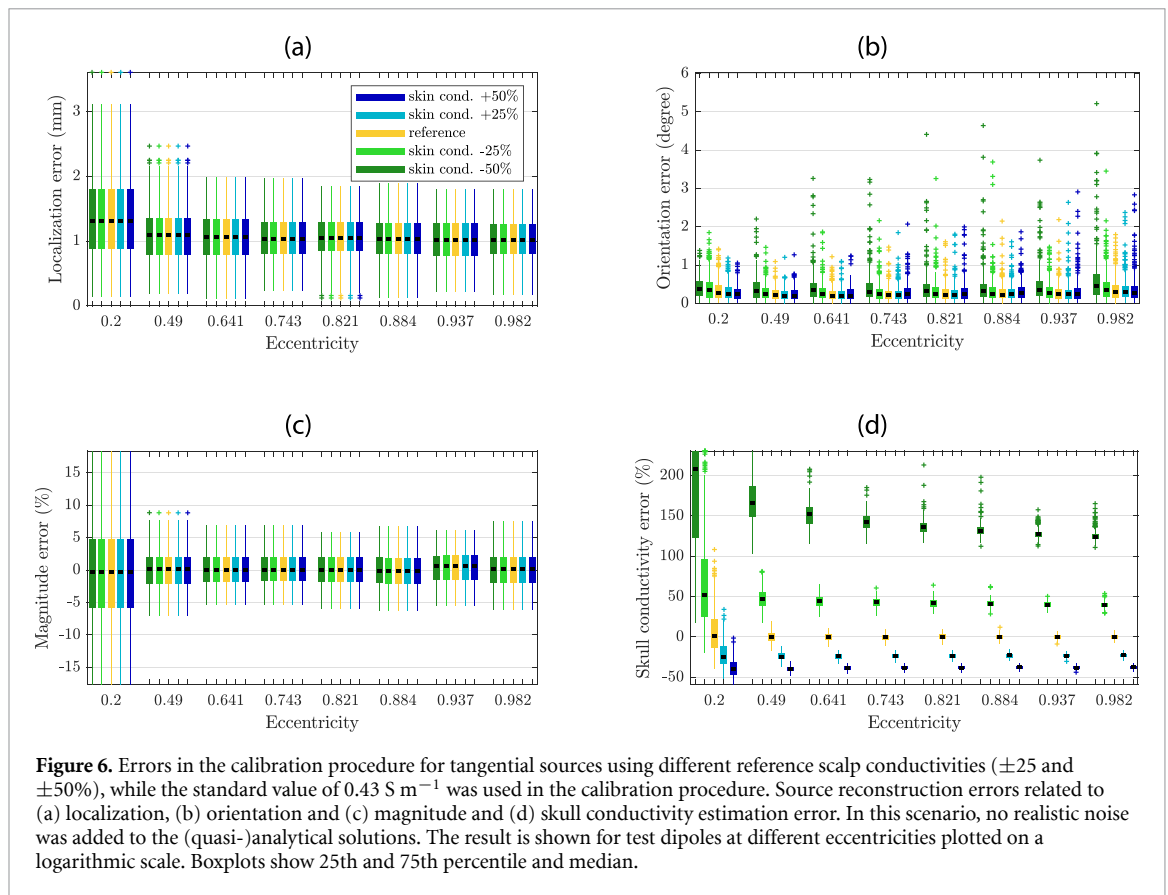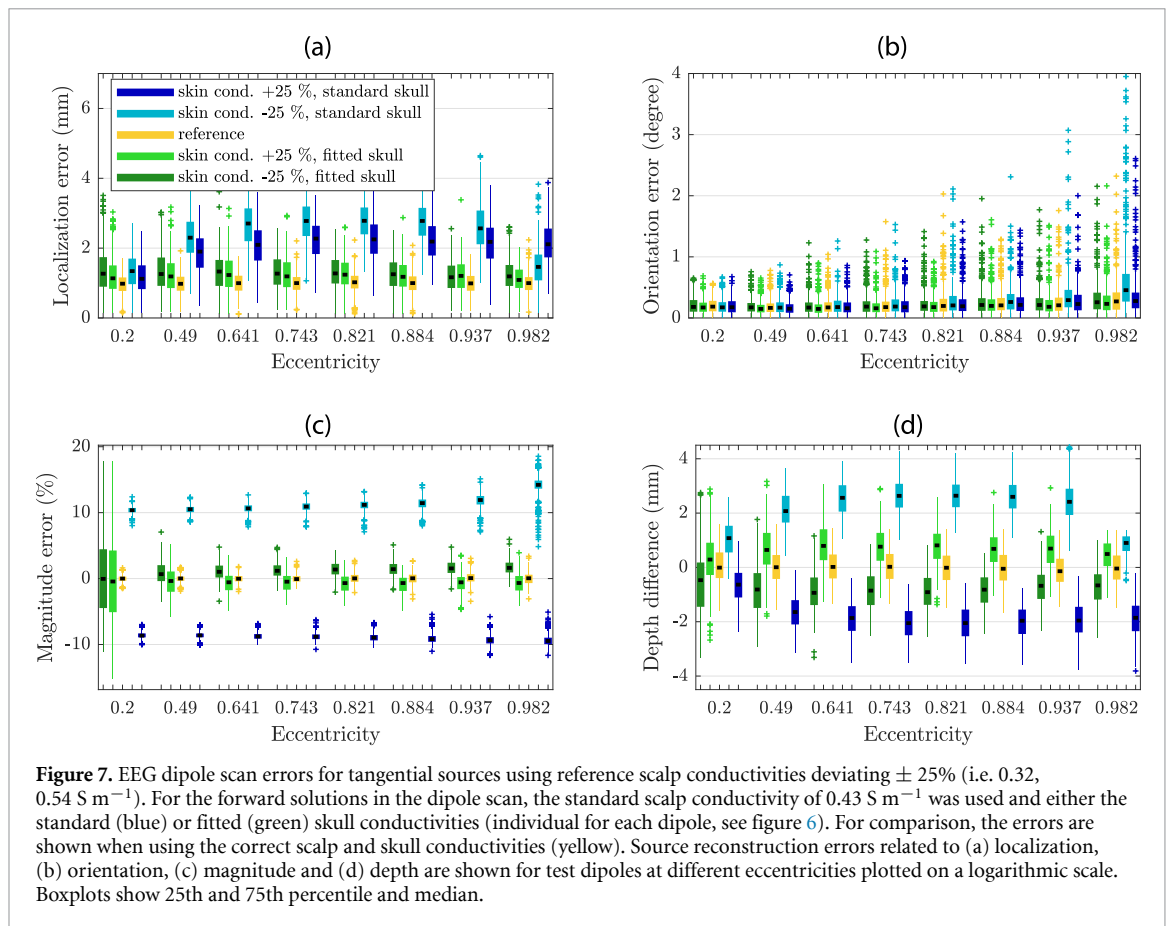
**Figure 6.** Errors in the calibration procedure for tangential sources using different reference scalp conductivities (±25 and ±50%), while the standard value of 0.43 S m⁻¹ was used in the calibration procedure. Source reconstruction errors related to (a) localization, (b) orientation and (c) magnitude and (d) skull conductivity estimation error. In this scenario, no realistic noise was added to the (quasi-)analytical solutions. The result is shown for test dipoles at different eccentricities plotted on a logarithmic scale. Boxplots show 25th and 75th percentile and median.

1.1° ± 0.6° (tangential), 1.1° ± 0.7° (25°) and 1.2° ± 0.8° (65°). The resulting mean skull conductivity errors (figure 5(d)) are 0.06% ± 5.4% (tangential), 0.1% ± 6.0% (25°) and 1.7% ± 14.2% (65°) at an eccentricity of 0.821. In the neighboring eccentricities, nearly identical errors can be observed. For EEG, the SNR (figure 5(e)) is almost unaffected by different orientations with a mean value of 7.0 (tangential, 25°) and 7.1 (65°) at 0.821. For MEG, higher SNRs can be observed for more tangential sources with mean values of 12.8 (tangential), 11.6 (25°) and 5.5 (65°). Note that for the deepest sources the calibration algorithm results in a negative magnitude, thus flipping the orientation obtained from the EEG fit, for 32 (65°) dipoles.

### 3.3. Influence of erroneous conductivities of other tissues

So far, we have assumed literature values for the compartments of scalp, CSF and brain. However, especially for the scalp compartment the conductivity is not known exactly and reported values vary (McCann *et al* 2019). Since the importance of the scalp conductivity has been emphasized in several studies as the second most important conductivity after skull conductivity (Vallaghé and Clerc 2009, Vorwerk *et al* 2019), we investigated the influence of wrongly assigned conductivity values for the scalp compartment on the proposed calibration procedure. For this purpose, the reference (in reality unknown) scalp conductivity value was increased or reduced by 25% or 50%, while the standard value of 0.43 S m⁻¹ was used in the calibration procedure. The results for the reconstructed dipole errors as well as the overall skull conductivity estimation error are depicted in figure 6.

All mean localization errors (figure 6(a)) lie below 1.4 mm with a maximal standard deviation of 0.6 mm, and are independent of conductivities. Similarly, the mean orientation errors (figure 6(b)) are below 0.6° with a maximal standard deviation of 0.6° and therefore also negligible. For the magnitude errors (figure 6(c)), the maximum mean is at 0.3%, the maximum standard deviation is 7.4%. For an eccentricity of 0.821, the skull conductivity estimation errors (figure 6(d)) are 136.4% ± 8.6% (41.9% ± 5.0%) if the actual scalp conductivity is 50% (25%) lower compared to the standard value, and −38.1% ± 2.2% (−23.4% ± 2.8%) if it is 50% (25%) higher that the standard scalp conductivity of 0.43 S m⁻¹ used in the estimation algorithm. In the neighboring eccentricities, similar errors can be observed. From a medical standpoint, we are not interested in the actual physical conductivity of the skull, but we are fitting this important parameter to achieve accurate source reconstructions using EEG and combined EEG/MEG. Thus, we evaluated the accuracy of an EEG single dipole deviation scan taking the uncertainty of scalp conductivity into account. For the reference solutions $M_{EEG}$, a higher (+25%) or lower (−25%) scalp conductivity

**Figure 7.** EEG dipole scan errors for tangential sources using reference scalp conductivities deviating $\pm 25\%$ (i.e. 0.32, 0.54 S m$^{-1}$). For the forward solutions in the dipole scan, the standard scalp conductivity of 0.43 S m$^{-1}$ was used and either the standard (blue) or fitted (green) skull conductivities (individual for each dipole, see figure 6). For comparison, the errors are shown when using the correct scalp and skull conductivities (yellow). Source reconstruction errors related to (a) localization, (b) orientation, (c) magnitude and (d) depth are shown for test dipoles at different eccentricities plotted on a logarithmic scale. Boxplots show 25th and 75th percentile and median.

compared to the standard value was used. In the calibration algorithm the standard value of 0.43 S m$^{-1}$ was used, thus, the real value was either under- or overestimated. In addition, either the standard skull conductivity or the fitted skull conductivity (see figure 6) was used. Figure 7 depicts the EEG source reconstruction errors when different scalp and skull conductivities are used. For comparison, the results are shown when using the correct scalp and skull conductivity in algorithm 1 (yellow).

It can be observed that using the standard values (over- or underestimating scalp conductivity by 25%), the localization error (figure 7(a)) is clearly higher when using the standard skull conductivity with mean values of 2.8 mm for overestimating (light blue) and 2.2 mm for underestimating (dark blue) scalp conductivity at eccentricity 0.821. These localization errors mainly translate into depth errors (figure 7(d)) and result in amplitude errors (figure 7(c)) of on average 11.1% (−8.9%) for overestimating (underestimating) scalp conductivity.

If the fitted skull conductivities are used, this effect can be alleviated, leading to mean localization errors of maximally 1.3 at the most relevant eccentricity for overestimating (dark green) and underestimating (light green) scalp conductivity. Note that on average, the test dipoles are 0.97 mm away from the closest source space node, see section 2.2.

## 4. Discussion

Although it has been shown that skull conductivity has a large impact on EEG source localization (Vorwerk *et al* 2019, Montes-Restrepo *et al* 2014, Gonçalves *et al* 2003, Baysal and Haueisen 2004, Huang *et al* 2007) as well as on TES (Saturnino *et al* 2019, Schmidt *et al* 2015), standard literature conductivity values are still most often used in the application fields. In this study, we presented a novel method for calibrating head volume conductor models in a continuous parameter range. It can take into account the inter-subject variability of bulk (calibrated) skull conductivity using only the non-invasive modalities EEG and MEG available in a standard MEG laboratory and for which ethical clearance is nowadays standard. Our new method can be used as follows. (a) One run of SEP and SEF data acquisition, to evoke the individual P20/N20 component. (b) The P20/N20 peak topographies are then used to individually calibrate the head volume conductor model. (c) This individualized head model can then be used for source analysis of EEG or combined EEG/MEG data of interest such as, for example, inter-ictal activity in presurgical epilepsy

diagnosis (Aydin *et al* 2017), or for an individual optimization of a multi-channel TES montage (Huang *et al* 2017, Guler *et al* 2016, Wagner *et al* 2016). In our algorithm, we use Brent's method to find the best fitting skull conductivity, which involves iterations using the golden section search and inverse parabolic fitting and which results in a higher accuracy using a comparable number of iterations compared to similar discrete approaches (Aydin *et al* 2014, Antonakakis *et al* 2019, 2020). By providing a complete mathematical description and an optimization method to iteratively update the skull conductivity parameter in order to find the best fitting value, we allow an automated calibration procedure which can easily be integrated into existing analysis pipelines. Therefore, the presented method is a promising new tool to provide an automatic pipeline to replace the standard models by individually calibrated head models that could lead to more reliable EEG or combined EEG/MEG source reconstruction results as well as improved optimized multi-channel TES montages in the future.

Our goal was to first validate and evaluate the new method in a controlled scenario, as done in the work at hand, by using a spherical head volume conductor model in which (quasi-)analytical expressions for the EEG and MEG solutions exist. Using this simplified setup, we can validate the algorithm in a fully controlled forward scenario, without interplay with numerical errors that are unavoidable in realistic head modeling setups. The proposed algorithm is validated and tested with regard to different levels of noise and typical source strengths from somatosensory experiments, different source depths and orientations, and inaccurate scalp conductivity assumptions.

First, in section 3.1, the source strengths resulting from different somatosensory experiments are compared using either Gaussian noise or prestimulus signals from a realistic measurement. Overall, the reference skull conductivity and source characteristics can be reliably reconstructed for sources similar to the generator of the P20/N20 response. Using prestimulus signal noise from an experimental measurement and tangential sources at an eccentricity of 0.821 which approximately corresponds to the P20/N20 source, the resulting mean estimated skull conductivity errors are 0.5% ± 10.9% for source strengths corresponding to electric wrist stimulation. Since realistic noise is correlated in time and space, we observe higher errors in the calibration algorithm when using baseline noise than we observe with white Gaussian noise with the same mean standard deviation per channel. This might be due to the high stimulation rate for the data we used here, where the somatosensory processing of trial $n-1$ is still going on, while trial $n$ starts to be processed (Antonakakis *et al* 2019). After averaging, the baseline might contain a remaining weak signal, possibly even produced by later components from the somatosensory network. Second, in section 3.2, the influence of different source orientations is examined, while noise with realistic strength is added to the (quasi-)analytical solutions. As in the previous scenario, the localization and magnitude errors, which are related to the MEG signal, become nearly constant for more eccentric sources and strongly increase for deeper sources. The reason for this is that the sensor level noise has a stronger effect for deeper sources, while the more eccentric sources can still be well identified. Note that the localization error is also bound by the 2 mm resolution of the source space, since the closest source space node is up to 1.66 mm away, while the average distance is 0.97 mm to avoid an inverse crime (Kaipio and Somersalo 2005). In a third study, see section 3.3, the influence of erroneous scalp conductivity is analyzed without artificial noise. The low localization errors mainly result from the resolution of the source space and the increasing numerical errors when computing the pseudo-inverse of the leadfield matrix for the dipole scan for deeper sources in case of MEG. No localization difference can be observed for the different conditions, since the MEG is unaffected by conductivities in a multi-layer sphere model. When performing an EEG single dipole deviation scan while over-/underestimating scalp conductivity, the errors are largely counterbalanced by our calibration approach, leading only to small localization errors. The opposite effect of scalp and skull conductivity on source depth has also been shown in Vorwerk *et al* (2019). Note that in our calibration algorithm only one free parameter is fitted, which is the most influential conductivity parameter, namely skull conductivity (Vorwerk *et al* 2019). However, as this scenario shows, the other conductivity values are indirectly taken into account, as we do not physically measure the skull resistivity, but rather fit this important parameter so that in combination with the other tissue conductivities, the data is best explained.

Our algorithm requires both EEG and MEG modalities to be experimentally available which may limit its applicability. However, the MEG is necessary for stabilizing the calibration procedure by fixing the source location, as calibration approaches using EEG alone (Lew *et al* 2009) have proven to be too unstable due to the correlation between source depth and skull conductivity. Additionally, further studies are needed to assess the stability and reliability in controlled scenarios using realistic head models.

As future outlook, our next step will therefore be to evaluate the new method in realistic head models using measured SEP/SEF data. This entails several challenges, e.g. there are different approaches to model the skull, ranging from a homogeneous tissue to a sandwich structure or even individually segmented spongy part of the cranial bone from imaging data (Antonakakis *et al* 2020, Montes-Restrepo *et al* 2014, McCann *et al* 2019). Additionally, since no analytical solutions exist for realistically shaped head models, the forward

solutions need to be computed numerically. Multiple methods to efficiently solve the EEG forward problem and to accurately model the source term have been proposed (Cuartas Morales *et al* 2019, Azizollahi *et al* 2018, Beltrachini 2019, Piastra *et al* 2018, Montes-Restrepo *et al* 2014). Moreover, in the realistic head model, the MEG might be affected by the conductivity profile of the tissues close to the source (Haueisen *et al* 1997). Skin and skull conductivities, however, which are the most influential material parameters on the EEG side (Vorwerk *et al* 2019), have nearly no influence on the MEG side also in a realistic head model (Lew *et al* 2013, Antonakakis *et al* 2019, Brette and Destexhe 2012, Haueisen *et al* 1997), except in the case of skull defects (Lau *et al* 2016). Therefore, in order to minimize the computational cost for the numerical calculations for a realistic head model, we suggest to carry out the MEG single dipole deviation scan in step 1 of algorithm 1 also only once to fix the source location (by using a standard skull conductivity for the realistic head model), very similar to the multi-layer sphere model and as done in Antonakakis *et al* (2019, 2020). This way, the computationally expensive MEG leadfield needs to be computed only once to fix the source location. Since we require the MEG forward solution for the entire source grid within the gray matter compartment, the transfer matrix approach is an efficient way to compute this leadfield (Wolters *et al* 2004). In step 2 of the algorithm, the source location is already fixed, so the EEG forward solution is only computed for this specific location, not the entire source grid. Therefore, we suggest not to use the transfer matrix approach, but instead compute the potential directly in this case. In addition to these measures, modern approaches to estimate the conductivity-dependent leadfield matrices using reduced order modeling approaches or hierarchical tensor formats in combination with leadfield interpolation techniques might further reduce the computational costs (Beltrachini 2017, Werthmann *et al* 2020). For the spherical case described in this study, we performed the entire pipeline in Matlab. For the future realistic head model studies, we intend to use the Matlab interface of the DUNEuro[7] toolbox for the forward calculations to allow an automated Matlab-based procedure as well. We believe that this will make the calibration procedure more applicable and user-friendly.

Additionally, further somatosensory experiments are needed to optimize the experimental parameters such as, for example, the stimulation rate so that a maximal P20/N20 SNR is accompanied by minimal remaining additive correlated noise, as can be estimated from the baseline.

A possible option to develop the calibration algorithm further might be to use the MEG data to determine not only the dipole location, but also the (quasi-)tangential orientation components of the source, and only rely on the EEG for the (quasi-)radial one (Huang *et al* 2007). This might be a possibility to further stabilize the method. Furthermore, alternatively (or also additionally) other SEP/SEF data (e.g. left and right wrist medianus or tibialis) or auditory evoked potentials/fields might be used for a further stabilization of the proposed calibration approach.

## 5. Conclusion

The aim of this study was to evaluate the accuracy of the proposed automatic calibration algorithm in the controlled setup of a multi-layer sphere model, i.e. without numerical errors, and under conditions which are as realistic as possible. In the presence of realistic noise levels and for dipole characteristics related to source reconstructions of SEP/SEF from electric wrist stimulation, the reference skull conductivity could be reliably reconstructed. In case of incorrect assumptions about the scalp conductivity, the algorithm resulted in a skull conductivity that counterbalanced this effect. EEG source reconstructions using the fitted skull conductivity parameter resulted in lower errors than when using the standard value. Future studies are required to validate the method in realistic head models with the aim to improve the individualization in EEG and combined EEG/MEG source analysis as well as in optimized multi-channel TES.

## ORCID iDs

S Schrader ● https://orcid.org/0000-0002-2402-5275
M Antonakakis ● https://orcid.org/0000-0003-1173-7895
S Rampp ● https://orcid.org/0000-0002-4826-1520
C Engwer ● https://orcid.org/0000-0002-6041-8228

[7] http://duneuro.org.

C H Wolters ⓘ https://orcid.org/0000-0001-6233-424X

# References

Abascal J-F P J, Arridge S R, Atkinson D, Horesh R, Fabrizi L, De Lucia M, Horesh L, Bayford R H and Holder D S 2008 Use of anisotropic modelling in electrical impedance tomography; description of method and preliminary assessment of utility in imaging brain function in the adult human head *Neuroimage* **43** 258–68

Akalin Acar Z, Acar C E and Makeig S 2016 Simultaneous head tissue conductivity and EEG source location estimation *Neuroimage* **124** 168–80

Akhtari M *et al* 2002 Conductivities of three-layer human skull *Brain Topogr.* **14** 151–67

Allison T, McCarthy G, Wood C C and Jones S J 1991 Potentials evoked in human and monkey cerebral cortex by stimulation of the median nerve. A review of scalp and intracranial recordings *Brain* **114** 2465–503

Antonakakis M, Schrader S, Aydin U, Khan A, Gross J, Zervakis M, Rampp S and Wolters C H 2020 Inter-subject variability of skull conductivity and thickness in calibrated realistic head models *Neuroimage* **223** 117353

Antonakakis M, Schrader S, Wollbrink A, Oostenveld R, Rampp S, Haueisen J and Wolters C H 2019 The effect of stimulation type, head modeling and combined EEG and MEG on the source reconstruction of the somatosensory P20/N20 component *Hum. Brain Mapp.* **40** 5011–28

Aydin U *et al* 2014 Combining EEG and MEG for the reconstruction of epileptic activity using a calibrated realistic volume conductor model *PLoS ONE* **9** e93154

Aydin U, Rampp S, Wollbrink A, Kugel H, Cho J-H, Knösche T R, Grova C, Wellmer J and Wolters C H 2017 Zoomed MRI guided by combined EEG/MEG source analysis: a multimodal approach for optimizing presurgical epilepsy work-up and its application in a multi-focal epilepsy patient case study *Brain Topogr.* **30** 417–33

Azizollahi H, Darbas M, Diallo M M, El Badia A and Lohrengel S 2018 EEG in neonates: forward modeling and sensitivity analysis with respect to variations of the conductivity *Math. Biosci. Eng.* **15** 905–32

Baysal U and Haueisen J 2004 Use of a priori information in estimating tissue resistivities—application to human data *in vivo Physiol. Meas.* **25** 737–48

Beltrachini L 2017 A reduced order modelling approach for fast generation of lead field matrices *2nd Int. Conf. on Basic and Clinical Multimodal Imaging (BACI 2017)* abstract num. 157

Beltrachini L 2019 The analytical subtraction approach for solving the forward problem in EEG *J. Neural Eng.* **16** 056029

Bikson M *et al* 2016 Safety of transcranial direct current stimulation: evidence based update 2016 *Brain Stimul.* **9** 641–61

Brent R P 1972 *Algorithms for Minimization Without Derivatives* (Englewood Cliffs, NJ: Prentice-Hall)

Brette R and Destexhe A 2012 *Handbook of Neural Activity Measurement* (Cambridge: Cambridge University Press) (https://doi.org/10.1017/CBO9780511979958)

Chen F, Hallez H and Staelens S 2010 Influence of skull conductivity perturbations on EEG dipole source analysis *Med. Phys.* **37** 4475–84

Cuartas Morales E, Acosta-Medina C D, Castellanos-Domínguez G and Mantini D 2019 A finite-difference solution for the EEG forward problem in inhomogeneous anisotropic media *Brain Topogr.* **32** 229–39

de Munck J C and Peters M J 1993 A fast method to compute the potential in the multisphere model (EEG application) *IEEE Trans. Biomed. Eng.* **40** 1166–74

Fernández-Corazza M, Turovets S, Luu P, Price N, Muravchik C H and Tucker D 2018 Skull modeling effects in conductivity estimates using parametric electrical impedance tomography *IEEE Trans. Biomed. Eng.* **65** 1785–97

Fuchs M, Wagner M, Wischmann H-A, Köhler T, Theißen A, Drenckhahn R and Buchner H 1998 Improving source reconstructions by combining bioelectric and biomagnetic data *Electroencephalogr. Clin. Neurophysiol.* **107** 93–111

Gonçalves S, de Munck J C, Verbunt J P A, Heethaar R M and da Silva F H L 2003 *In vivo* measurement of the brain and skull resistivities using an EIT-based method and the combined analysis of SEF/SEP data *IEEE Trans. Biomed. Eng.* **50** 1124–7

Guler S, Dannhauer M, Erem B, MacLeod R, Tucker D, Turovets S, Luu P, Erdogmus D and Brooks D H 2016 Optimization of focality and direction in dense electrode array transcranial direct current stimulation (tDCS) *J. Neural Eng.* **13** 036020

Götz T, Huonker R, Witte O W and Haueisen J 2014 Thalamocortical impulse propagation and information transfer in EEG and MEG *J. Clin. Neurophysiol.* **31** 253–60

Haueisen J, Ramon C, Eiselt M, Brauer H and Nowak H 1997 Influence of tissue resistivities on neuromagnetic fields and electric potentials studied with a finite element model of the head *IEEE Trans. Biomed. Eng.* **44** 727–35

Hoekema R, Wieneke G H, Leijten F S S, van Veelen C W M, van Rijen P C, Huiskamp G J M, Ansems J and van Huffelen A C 2003 Measurement of the conductivity of skull, temporarily removed during epilepsy surgery *Brain Topogr.* **16** 29–38

Huang M-X *et al* 2007 A novel integrated MEG and EEG analysis method for dipolar sources *Neuroimage* **37** 731–48

Huang Y *et al* 2017 Measurements and models of electric fields in the *in vivo* human brain during transcranial electric stimulation *eLife* **6** e18834

Kaipio J P and Somersalo E 2005 *Statistical and Computational Inverse Problems* 1st edn vol 160 (New York: Springer) (https://doi.org/10.1007/b138659)

Lai Y, van Drongelen W, Ding L, Hecox K E, Towle V L, Frim D M and He B 2005 Estimation of *in vivo* human brain-to-skull conductivity ratio from simultaneous extra- and intra-cranial electrical potential recordings *Clin. Neurophysiol.* **116** 456–65

Lau S, Güllmar D, Flemming L, Grayden D B, Cook M J, Wolters C H and Haueisen J 2016 Skull defects in finite element head models for source reconstruction from magnetoencephalography signals *Front. Neurosci.* **10** 141

Lew S, Sliva D D, Choe M-S, Grant P E, Okada Y, Wolters C H and HämÄläinen M S 2013 Effects of sutures and fontanels on meg and eeg source analysis in a realistic infant head model *Neuroimage* **76** 282–93

Lew S, Wolters C H, Anwander A, Makeig S and MacLeod R 2009 Improved EEG source analysis using low-resolution conductivity estimation in a four-compartment finite element head model *Hum. Brain Mapp.* **30** 2862–78

Li X, Yu K and He B 2016 Magnetoacoustic tomography with magnetic induction (MAT-MI) for imaging electrical conductivity of biological tissue: a tutorial review *Phys. Med. Biol.* **61** R249–R270

McCann H, Pisano G and Beltrachini L 2019 Variation in reported human head tissue electrical conductivity values *Brain Topogr.* **32** 825–58

Montes-Restrepo V, van Mierlo P, Strobbe G, Staelens S, Vandenberghe S and Hallez H 2014 Influence of skull modeling approaches on EEG source localization *Brain Topogr.* **27** 95–111

Nakamura A, Yamada T, Goto A, Kato T, Ito K, Abe Y, Kachi T and Kakigi R 1998 Somatosensory homunculus as drawn by MEG *Neuroimage* **7** 377–86

Nissinen A, Kaipio J P, Vauhkonen M and Kolehmainen V 2015 Contrast enhancement in EIT imaging of the brain *Physiol. Meas.* **37** 1–24

Piastra M C, Nüßing A, Vorwerk J, Bornfleth H, Oostenveld R, Engwer C and Wolters C H 2018 The discontinuous Galerkin finite element method for solving the MEG and the combined MEG/EEG forward problem *Front. Neurosci.* **12** 30

Ramon C, Schimpf P, Haueisen J, Holmes M and Ishimaru A 2004 Role of soft bone, CSF and gray matter in EEG simulations *Brain Topogr.* **16** 245–8

Roche-Labarbe N, Aarabi A, Kongolo G, Gondry-Jouet C, Dümpelmann M, Grebe R and Wallois F 2008 High-resolution electroencephalography and source localization in neonates *Hum. Brain Mapp.* **29** 167–76

Sadleir R J, Vannorsdall T D, Schretlen D J and Gordon B 2012 Target optimization in transcranial direct current stimulation *Front. Psychiatry* **3** 90

Sarvas J 1987 Basic mathematical and electromagnetic concepts of the biomagnetic inverse problem *Phys. Med. Biol.* **32** 11–22

Saturnino G B, Thielscher A, Madsen K H, Knösche T R and Weise K 2019 A principled approach to conductivity uncertainty analysis in electric field calculations *Neuroimage* **188** 821–34

Schmidt C, Wagner S, Burger M, van Rienen U and Wolters C H 2015 Impact of uncertain head tissue conductivity in the optimization of transcranial direct current stimulation for an auditory target *J. Neural Eng.* **12** 046028

Stinstra J G and Peters M J 1998 The volume conductor may act as a temporal filter on the ECG and EEG *Med. Biol. Eng. Comput.* **36** 711–16

Tang C, You F, Cheng G, Gao D, Fu F and Dong X 2009 Modeling the frequency dependence of the electrical properties of the live human skull *Physiol. Meas.* **30** 1293–301

Tang C, You F, Cheng G, Gao D, Fu F, Yang G and Dong X 2008 Correlation between structure and resistivity variations of the live human skull *IEEE Trans. Biomed. Eng.* **55** 2286–92

Vallaghé S and Clerc M 2009 A global sensitivity analysis of three- and four-layer EEG conductivity models *IEEE Trans. Biomed. Eng.* **56** 988–95

Vorwerk J, Aydin U, Wolters C H and Butson C R 2019 Influence of head tissue conductivity uncertainties on EEG dipole reconstruction *Front. Neurosci.* **13** 531

Wagner S, Burger M and Wolters C H 2016 An optimization approach for well-targeted transcranial direct current stimulation *SIAM J. Appl. Math.* **76** 2154–74

Wendel K, Väisänen J, Seemann G, Hyttinen J and Malmivuo J 2010 The influence of age and skull conductivity on surface and subdermal bipolar EEG leads *Comput. Intell. Neurosci.* **2010** 397272

Werthmann T A, Wolters C H and Grasedyck L 2020 Approximation of parameter-dependent leadfield matrices using tensor formats *Workshop Biosignalverarbeitung 2020, Gemeinsamer Workshop der Fachausschüsse 'Biosignale' und 'Magnetische Methoden in der Medizin' der DGBMT im VDE*

Wolters C H, Beckmann R F, Rienäcker A and Buchner H 1999 Comparing regularized and non-regularized nonlinear dipole fit methods: a study in a simulated sulcus structure *Brain Topogr.* **12** 3–18

Wolters C H, Grasedyck L and Hackbusch W 2004 Efficient computation of lead field bases and influence matrix for the fem-based eeg and meg inverse problem *Inverse Probl.* **20** 1099–116

Wolters C H, Lew S, MacLeod R S and Hämäläinen M S 2010 Combined EEG/MEG source analysis using calibrated finite element head models *BiomedTech* (Suppl. 1) **55** 64–7